



OPEN

Magneto-hydrodynamic peristaltic flow of a Jeffery fluid in the presence of heat transfer through a porous medium in an asymmetric channel

A. M. Abd-Alla¹✉, S. M. Abo-Dahab², Doaa. M. Salah¹, F. S. Bayones³ & M. A. Abdelhafez¹

In the present paper, the effects of magnetic field and heat transfer on the peristaltic flow of a Jeffery fluid through a porous medium in an asymmetric channel have been studied. The governing non-linear partial differential equations representing the flow model are transmuted into linear ones by employing the appropriate non-dimensional parameters under the assumption of long wavelength and low Reynolds number. Exact solutions are presented for the stream function, pressure gradient, and temperature. The frictional force and pressure rise are both computed using numerical integration. Using MATLAB R2023a software, a parametric analysis is performed, and the resulting data is represented graphically. For all physical quantities considered, numerical calculations were made and represented graphically. Trapping phenomena are discussed graphically. The obtained results can be applied to enhance pumping systems in engineering and gastrointestinal functions. This analysis permits body fluids such as blood and lymph to easily move inside the arteries and veins, allowing oxygen supply, waste elimination, and other necessary elements.

List of symbols

α_1, γ_1	Amplitudes of the wavy walls
a, b	Amplitude ratios
$\alpha_1 + \alpha_2$	Width of channel
λ	Wavelength
c	Wave speed
t'	Time
u	Axial velocity
B_0	Intensity of external magnetic field
ρ	Constant density
g	Acceleration due to gravity
K	Thermal conductivity
c_p	Specific heat
M	Hartmann number
P	Pressure
u', v'	Velocity components in wave frame
μ_0	Constant viscosity
R	Thermal radiation parameter
σ	Electrical conductivity of the fluid
Re	Reynolds number
Gr	Grashof number
β	Heat source/sink parameter
θ	Temperature distribution

¹Department of Mathematics, Faculty of Science, Sohag University, Sohag, Egypt. ²Department of Mathematics, Faculty of Science, South Valley University, Qena 83523, Egypt. ³Department of Mathematics and Statistics, College of Science, Taif University, P. O. Box 11099, 21944 Taif, Saudi Arabia. ✉email: mohmrr@yahoo.com

Da Darcy's number
 Q_0 Heat source

Peristaltic transport has become a prominent topic for academics in recent years due to its use in physics, applied mathematics, physiology, engineering, various hose pumps, etc. Peristalsis is defined as a series of muscle relaxations and contractions of a blood vessel wall that push materials forward in fluid through tubules in a wave-like motion without an interface with the pump parts. Peristaltic movement can be observed during the passage of food through the stomach, esophagus, and intestines, through the blood in the arteries, veins, and capillaries, the exit of urine through the ureters from the kidney to the bladder, the movement of the egg and embryo in the tubes, and so on. Toxic fluids are transported in nuclear facilities using the peristaltic phenomenon. Such biomedical applications motivate the researchers and, therefore, many theoretical investigations have been tackled to see the impact of magnetic field on peristaltic flows^{1–4}. A porous medium is the matter which contains a number of small holes distributed throughout it. The fluid transport through porous medium is widely applicable in the vascular beds, lungs, kidneys, tumorous vessels, bile duct, gall bladder with stones, and small blood vessels. Some scientists contributed to study and develop the peristaltic flow through a porous medium^{5–8}. Latham⁹ studied the peristaltic mechanism to investigate urine flow through the ureter. In these days, the endoscope is a very significant tool utilize for analysing causes responsible for various complication in the organs of human in which the fluid is carried by peristaltic pumping like stomach and small intestine. There is no difference between catheter and an endoscope from dynamic point of view. Furthermore, the injection of a catheter will change the distribution and flow field in an artery¹⁰. Electroosmotic transport is a vital concern in microfluidics because of its applications in healthcare research, scientific and biological analysis, cardiac output challenges, medicine, and the treatment of aberrant and sickle cell diseases^{11–14}. Nanoparticle research is a topic of intense scientific interest due to the wide variety of possible applications in the biological, optical, and electrical fields. Nanoparticle examination is in the blink of an eye a region of effective experimental enthusiasm because of a gigantic scope of potential applications in electronic, optical, biomedical field. These tiny particles are mostly found in the metals such as nitrides, Carbides or non-metals (Graphite, Carbon nanotubes), nitrides^{15–21}. Ayub and Shahzadi²² analyzed a ballon model with Cu-blood medicated nanoparticles as drug agent through overlapped curved stenotic artery having compliant walls. Due to their wide range of industrial and engineering applications, such as the sketch of plastic films, food mixing, nuclear waste storage, aerodynamics, composite materials, paper and milk production, metal spinning processes, petroleum production, and many others, non-Newtonian liquids have seen a significant increase in interest in recent years. This inspired the development of several fluid flow, material analysis, and nanomaterials models^{23–28}. The bio-convected phenomena occurs due to the upward average movement of microorganisms that are denser in comparison to base-liquids such as water. The aggregation of microorganisms disrupted the suspension of surface by its increased density. This procedure resulted in microorganism tumbling and bio-convection current generation. The motivation for studying bioconvective phenomena in nanomaterials in view of such novel restrictions is to manage the transport process, which is required in engineering and industrial operations. For more details, see^{29–32}. Different pragmatic applications experience the flow through a permeable medium especially in geophysical fluid dynamics. Limestone, Sandstone, gall bladder with stones in tiny blood vessels, beach sand, bile duct and the human lung are the important examples of natural porous media^{33–38}. Few researchers have developed reduced graphene oxide–metal oxide composite gas sensors with excellent electrical and gas-sensing capabilities. However, it is still a relatively unexplored territory. Kiran Kumar et al.³⁹ provides an overview of electrical and gas-sensing properties of reduced graphene oxide–metal oxide nanocomposites with improved sensitivity, selectivity, stability, and other sensing performances. As the importance of heat transfer on peristaltic flow in porous media, many attempts have been made by researchers and scientists to study and develop peristaltic transfer due to its inclusion in many important applications. In addition, engineers use finger and roller pumps that operate on the peristaltic principle.^{40–41} discussed the heat transfer and magnetic field on the peristaltic flow. Many industrial and biological instruments, such as cylinder pumps, finger pumps, heart–lung machines, blood pump machines, and dialysis machines, are designed on the basis of the peristaltic mechanism. Recently, Abd-Alla et al.⁴² investigated the effect of heat and mass transfer on the nanofluid of peristaltic flow in a ciliated tube. In Refs.^{43–51}, peristaltic flow with new parameters with or without endoscope has been discussed.

The motivation of this paper is to study the magneto-hydrodynamic peristaltic flow of a Jeffery fluid in the presence of heat transfer through a porous medium in an asymmetric channel. Here we examine the impact of magnetic field and heat transfer on peristaltic flow an asymmetric channel. The aim of this paper is to demonstrate the effect of the porosity of the porous medium, thermal radiation, Darcy number and magnetic field in an asymmetric channel. Significant modelling is conferred with the aid of dimensionless parameters and using approximation of low Reynolds number and long wavelength to obtain linearized system of coupled differential equations which are then solved analytically. Finally, the detailed computational results are compiled and discussed with the physical interpretation of our results. The graphical upshots for the velocity, temperature, concentration, the gradient pressure, pressure rise and the friction force are examined for influential parameters. Results acquired from this examination provide a useful understanding and new visions about the particular nature of the peristalsis. Finally, the numerical result displayed by figures and the physical meaning is explained.

Formulation of the problem

Assume we have an asymmetric vertical channel of width $\alpha_1 + \alpha_2$ in a porous space for an incompressible Jeffrey fluid in the presence of heat when subjected to a magnetic field. The physical model of the problem and the flow coordinate system are shown in Fig. 1. The geometry of peristalsis's walls is defined as

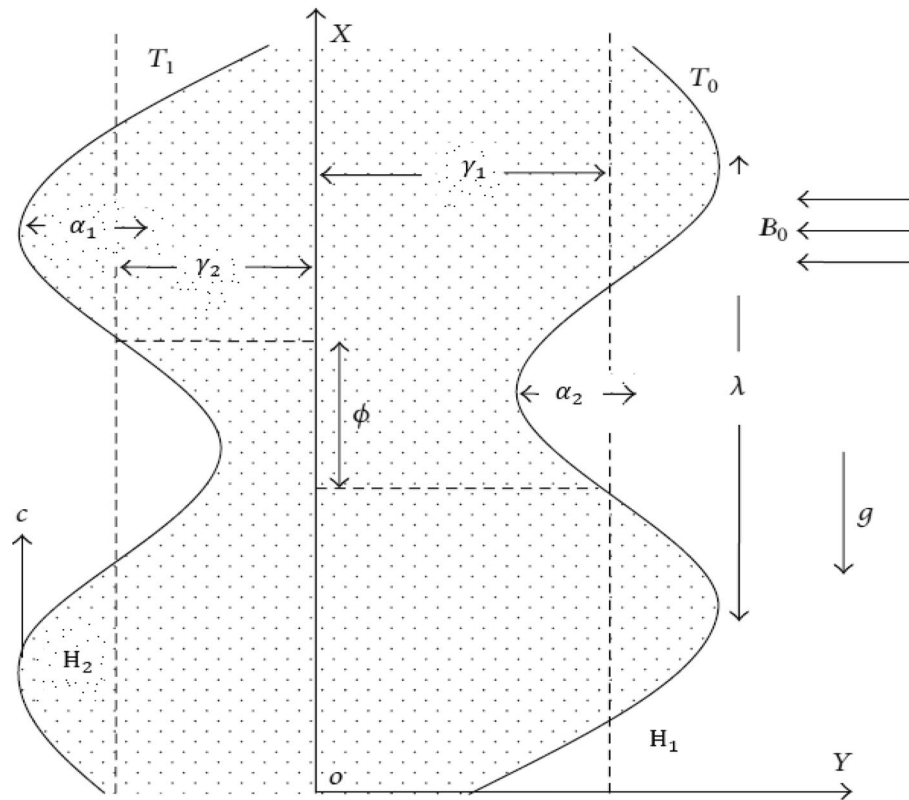


Figure 1. Diagrammatic depiction of the physical model.

$$H_1(X, t) = \alpha_1 + \gamma_1 \cos \left[\frac{2\pi}{\lambda} (X - ct) \right], \text{ upper wall,}$$

$$H_2(X, t) = -\alpha_2 - \gamma_2 \cos \left[\frac{2\pi}{\lambda} (X - ct) + \phi \right], \text{ lower wall,} \quad (1)$$

where the higher and lower waves' amplitudes, respectively, are γ_1, γ_2 , λ is the wavelength, t time, ϕ is the phase difference belongs to $[0, \pi]$. Furthermore, $\alpha_1, \alpha_2, \gamma_1, \gamma_2$ and ϕ satisfy the inequality below:

$$\gamma_1^2 + \gamma_2^2 + 2\gamma_1\gamma_2\cos\phi \leq (\alpha_1 + \alpha_2)^2. \quad (2)$$

The governing equations in the laboratory frame are^{7,8}

$$\frac{\partial U}{\partial X} + \frac{\partial V}{\partial Y} = 0,$$

$$\rho \left(U \frac{\partial U}{\partial X} + V \frac{\partial V}{\partial Y} \right) = -\frac{\partial P}{\partial X} + \frac{1}{\epsilon} \frac{\partial \tau_{xx}}{\partial X} + \frac{1}{\epsilon} \frac{\partial \tau_{xy}}{\partial Y} - \frac{\mu_0}{k} U + \rho g \alpha_T (T - T_0) - \sigma B_0^2 U,$$

$$\rho \left(U \frac{\partial U}{\partial X} + V \frac{\partial V}{\partial Y} \right) = -\frac{\partial P}{\partial Y} + \frac{1}{\epsilon} \frac{\partial \tau_{yx}}{\partial X} + \frac{1}{\epsilon} \frac{\partial \tau_{yy}}{\partial Y} - \frac{\mu_0}{k} V,$$

$$\rho c_p \left(U \frac{\partial}{\partial X} + V \frac{\partial}{\partial Y} \right) T = K \left(\frac{\partial^2}{\partial X^2} + \frac{\partial^2}{\partial Y^2} \right) T + Q_0 - \frac{\partial q}{\partial y}.$$

The relationships between the two frames are defined as follows:

$$x = X - ct, Y = y, u = U - c, v = V, p(x) = P(X, t), \quad (3)$$

where (u, v) , (U, V) , (p, P) and T represent the components of velocity in the wave frame of reference, the velocity components in laboratory frame, the pressure in wave and fixed frame and, the temperature respectively. Since a small Reynolds number is assumed, the induced magnetic field is ignored.

Following are the basic equations used to explain the flow field:

$$\frac{\partial u}{\partial x} + \frac{\partial v}{\partial y} = 0, \tag{4}$$

$$\rho \left((u + c) \frac{\partial u}{\partial x} + v \frac{\partial v}{\partial y} \right) = -\frac{\partial p}{\partial x} + \frac{1}{\epsilon} \frac{\partial \tau_{xx}}{\partial x} + \frac{1}{\epsilon} \frac{\partial \tau_{xy}}{\partial y} - \frac{\mu^\circ}{k} (u + c) + \rho g \alpha_T (T - T_\circ) - \sigma B_\circ^2 (u + c), \tag{5}$$

$$\rho \left(u \frac{\partial u}{\partial x} + v \frac{\partial v}{\partial y} \right) = -\frac{\partial p}{\partial y} + \frac{1}{\epsilon} \frac{\partial \tau_{yx}}{\partial x} + \frac{1}{\epsilon} \frac{\partial \tau_{yy}}{\partial y} - \frac{\mu^\circ}{k} v, \tag{6}$$

$$\rho c_p \left((u + c) \frac{\partial}{\partial x} + v \frac{\partial}{\partial y} \right) T = \left(\frac{\partial^2}{\partial x^2} + \frac{\partial^2}{\partial y^2} \right) T + Q_\circ - \frac{\partial q}{\partial y}, \tag{7}$$

where

$$\begin{aligned} \tau_{xx} &= \frac{2\mu^\circ}{1 + \lambda_1} \left[1 + \lambda_2 \left((u + c) \frac{\partial}{\partial x} + v \frac{\partial}{\partial y} \right) \right] \frac{\partial u}{\partial x}, \\ \tau_{xy} &= \frac{2\mu^\circ}{1 + \lambda_1} \left[1 + \lambda_2 \left((u + c) \frac{\partial}{\partial x} + v \frac{\partial}{\partial y} \right) \right] \left(\frac{\partial u}{\partial y} + \frac{\partial v}{\partial x} \right), \\ \tau_{yy} &= \frac{2\mu^\circ}{1 + \lambda_1} \left[1 + \lambda_2 \left((u + c) \frac{\partial}{\partial x} + v \frac{\partial}{\partial y} \right) \right] \frac{\partial v}{\partial y}. \end{aligned} \tag{8}$$

In the above equations k is the permeability of the porous medium, Q_\circ is the heat source, λ_1 is the ratio of relaxation to retardation times, λ_2 is the retardation time, ρ is the density, K_1 is the thermal conductivity, σ is the electrical conductivity of the fluid, c_p is the specific heat, q is the radiative heat flux and ϵ is the porosity of the porous medium and B_\circ is the applied magnetic field. The non-dimensional quantities are given below:

$$\begin{aligned} x = \frac{\bar{x}}{\lambda}, y = \frac{\bar{y}}{\alpha_1}, u = \frac{\bar{u}}{c}, v = \frac{\bar{v}}{c\delta}, h_1 = \frac{H_1}{\alpha_1}, h_2 = \frac{H_2}{\alpha_1}, \tau = \frac{a_1 \bar{\tau}}{\mu^\circ c}, t = \frac{c \bar{t}}{\lambda}, Da = \frac{k}{\alpha_1^2}, \delta = \frac{\alpha_1}{\lambda}, \\ p = \frac{\alpha_1^2 \bar{p}}{\mu^\circ \lambda c}, a = \frac{\gamma_1}{\alpha_1}, b = \frac{\gamma_2}{\alpha_1}, d = \frac{\alpha_2}{\alpha_1}, Gr = \frac{\rho g \alpha_T \alpha_1^2 (T_1 - T_\circ)}{\mu^\circ c}, Re = \frac{\rho c \alpha_1}{\mu^\circ}, \theta = \frac{\bar{T} - \bar{T}_\circ}{T_1 - T_\circ}, \\ \beta = \frac{Q_\circ \alpha_1^2}{k(T_1 - T_\circ)}, M = \sqrt{\frac{\sigma}{\mu^\circ} B_\circ \alpha_1}, q = -RK_1 \frac{\partial T}{\partial y}. \end{aligned} \tag{9}$$

Applying (9) in (1) and (4)–(8) and illuminate the bars, we have,

$$\frac{\partial u}{\partial x} + \frac{\partial v}{\partial y} = 0, \tag{10}$$

$$Re\delta \left((u + 1) \frac{\partial u}{\partial x} + v \frac{\partial v}{\partial y} \right) = -\frac{\partial p}{\partial x} + \frac{\delta}{\epsilon} \frac{\partial \tau_{xx}}{\partial x} + \frac{1}{\epsilon} \frac{\partial \tau_{xy}}{\partial y} - \frac{1}{Da} (u + 1) + Gr\theta - M^2 (u + 1), \tag{11}$$

$$Re\delta^3 \left((u + 1) \frac{\partial v}{\partial x} + v \frac{\partial v}{\partial y} \right) = -\frac{\partial p}{\partial y} + \frac{\delta^2}{\epsilon} \frac{\partial \tau_{xy}}{\partial x} + \frac{\delta}{\epsilon} \frac{\partial \tau_{yy}}{\partial y} - \frac{\delta^2}{Da} v, \tag{12}$$

$$\rho c_p \frac{c\delta}{a_1} \left((u + 1) \frac{\partial}{\partial x} + v \frac{\partial}{\partial y} \right) \theta (T_1 - T_\circ) = \left(\frac{\delta^2}{a_1^2} \frac{\partial^2}{\partial x^2} + \frac{1}{a_1^2} \frac{\partial^2}{\partial y^2} \right) \theta (T_1 - T_\circ) + Q_\circ + \frac{Rk}{a_1^2} (T_1 - T_\circ) \frac{\partial^2 \theta}{\partial y^2}, \tag{13}$$

$$\tau_{xx} = \frac{2\delta}{1 + \lambda_1} \left[1 + \frac{\lambda_2 c \delta}{a_1} \left((u + 1) \frac{\partial}{\partial x} + v \frac{\partial}{\partial y} \right) \right] \frac{\partial u}{\partial x},$$

$$\tau_{xy} = \frac{1}{1 + \lambda_1} \left[1 + \frac{\lambda_2 c \delta}{a_1} \left((u + 1) \frac{\partial}{\partial x} + v \frac{\partial}{\partial y} \right) \right] \left(\frac{\partial u}{\partial y} + \delta^2 \frac{\partial v}{\partial x} \right),$$

$$\tau_{yy} = \frac{2\delta}{1 + \lambda_1} \left[1 + \frac{\lambda_2 c \delta}{a_1} \left((u + 1) \frac{\partial}{\partial x} + v \frac{\partial}{\partial y} \right) \right] \frac{\partial v}{\partial y}, \tag{14}$$

$$\tilde{h}_1 = 1 + a \cos 2\pi x, \tilde{h}_2 = -d - b \cos(2\pi x + \varnothing).$$

From (11), (12) and (13) and by ignoring terms containing δ and its higher powers by utilizing the long wavelength approximation ($\delta \ll 1$) and low Reynolds number assumption, we have

$$\frac{\partial p}{\partial x} = \frac{1}{\epsilon} \frac{\partial}{\partial y} \left[\frac{1}{1 + \lambda_1} \frac{\partial u}{\partial y} \right] - \frac{1}{Da} (u + 1) + Gr\theta - M^2(u + 1), \tag{15}$$

and

$$\frac{\partial p}{\partial y} = 0, \tag{16}$$

$$\frac{d^2\theta}{dy^2} + N_1 = 0. \tag{17}$$

According to Eq. (16), p is not dependent on y . Consequently, (15) may be expressed as

$$\frac{dp}{dx} = \frac{1}{\epsilon} \frac{\partial}{\partial y} \left[\frac{1}{1 + \lambda_1} \frac{\partial u}{\partial y} \right] - \left(\frac{1}{Da} + M^2 \right) (u + 1) + Gr\theta, \tag{18}$$

These non-dimensional boundary conditions are^{40,41} equivalent to

$$\begin{aligned} u &= -1, \text{ at } y = \tilde{h}_1, \tilde{h}_2, \\ \theta &= 1, \text{ at } y = \tilde{h}_1, \tilde{h}_2. \end{aligned} \tag{19}$$

According to the wave frame, the volumetric flow rate in the non-dimensional form is

$$F = \int_{\tilde{h}_2}^{\tilde{h}_1} u dy. \tag{20}$$

Solution of the problem

We get θ and u by solving (15), (17), and applying the boundary conditions (19).

$$\theta = \frac{2\tilde{h}_1 - 2y - \tilde{h}_1^2 N_1 + \tilde{h}_1 \tilde{h}_2^2 N_1 + \tilde{h}_1^2 y N_1}{2(\tilde{h}_1 - \tilde{h}_2)}, \tag{21}$$

$$\begin{aligned} u &= b_0 e^{-\sqrt{A_2}y} \left\{ b_1 + b_2 e^{2\sqrt{A_2}y} + b_4 \left(b_3 - e^{\sqrt{A_2}(2\tilde{h}_1+y)} + e^{\sqrt{A_2}(2\tilde{h}_2+y)} + e^{\sqrt{A_2}(\tilde{h}_1+2y)} - e^{\sqrt{A_2}(\tilde{h}_2+2y)} \right) \right. \\ &\quad \left. + b_5 + b_6 e^{\sqrt{A_2}(\tilde{h}_1+2y)} + b_7 (\tilde{h}_1 - y) (b_8 + b_9 y) \left(e^{\sqrt{A_2}(2\tilde{h}_2+y)} - e^{\sqrt{A_2}(2\tilde{h}_1+y)} \right) \right\}, \end{aligned} \tag{22}$$

where $N_1 = \frac{\beta}{1+R}$, $b_0 = \frac{1}{2A_2^2(e^{2\sqrt{A_2}\tilde{h}_1} - e^{2\sqrt{A_2}\tilde{h}_2})}$, $b_1 = -2A_2^2 e^{2\sqrt{A_2}(\tilde{h}_1+\tilde{h}_2)} (e^{\sqrt{A_2}\tilde{h}_1} - e^{\sqrt{A_2}\tilde{h}_2})$, $b_2 = -2A_2^2$

$$(e^{\sqrt{A_2}\tilde{h}_1} - e^{\sqrt{A_2}\tilde{h}_2}), b_3 = (e^{\sqrt{A_2}(2\tilde{h}_1+\tilde{h}_2)} - e^{\sqrt{A_2}(\tilde{h}_1+2\tilde{h}_2)}),$$

$$b_4 = 2A_3(\tilde{h}_1 - \tilde{h}_2)^2 N_1 + 2A_1 A_2, b_5 = -2A_2 A_3 (\tilde{h}_1 - \tilde{h}_2)^2 e^{\sqrt{A_2}(2\tilde{h}_1+\tilde{h}_2)},$$

$$b_6 = 2A_2 A_3 (\tilde{h}_1 - \tilde{h}_2)^2, b_7 = -A_2 A_3 (\tilde{h}_1 - \tilde{h}_2), b_8 = 2 - \tilde{h}_1 \tilde{h}_2 N_1 + \tilde{h}_2^2 N_1, b_9 = (\tilde{h}_1 - \tilde{h}_2) N_1,$$

$$m = \epsilon(1 + \lambda_1), A_1 = m \left(\frac{\partial p}{\partial x} + \frac{1}{Da} + M^2 \right), A_2 = m \left(\frac{1}{Da} + M^2 \right), A_3 = mGr.$$

It follows from (22) and (20) that the pressure gradient can be written as

$$\begin{aligned} \frac{dp}{dx} &= \frac{1}{v_2} \left[F + \sqrt{A_2} b_0 (b_1 - b_2 + b_5) e^{-\sqrt{A_2}(\tilde{h}_1-\tilde{h}_2)} - \sqrt{A_2} b_0 b_6 e^{\sqrt{A_2}\tilde{h}_1} + b_{10} \tilde{h}_2 (b_8 + b_9(\tilde{h}_1 - \tilde{h}_2))(1 - b_9) \right] \\ &\quad - \left(\frac{1}{Da} + M^2 \right), \end{aligned} \tag{23}$$

where $b_{10} = b_7(e^{2\sqrt{A_2}\bar{h}_2} - e^{2\sqrt{A_2}\bar{h}_1})$, $v_1 = \sqrt{A_2}b_0b_3e^{-\sqrt{A_2}(\bar{h}_1-\bar{h}_2)} + \sqrt{A_2}b_0[e^{\sqrt{A_2}(2\bar{h}_1-\bar{h}_2)} - e^{\sqrt{A_2}\bar{h}_1}] - b_0(\bar{h}_1 - \bar{h}_2)e^{2\sqrt{A_2}\bar{h}_1} + b_0(\bar{h}_1 - \bar{h}_2)e^{2\sqrt{A_2}\bar{h}_2}$, $v_2 = 2mA_2v_1$.

Based on (23) we have the pressure rise Δp_λ per one wavelength and the friction force for the upper and lower wall F_λ^u, F_λ^l as follow:

$$\Delta p_\lambda = \int_0^1 \left(\frac{dp}{dx}\right) dx, F_\lambda^u = \int_0^1 \bar{h}_1^2 \left(\frac{-dp}{dx}\right) dx \text{ and } F_\lambda^l = \int_0^1 \bar{h}_2^2 \left(\frac{-dp}{dx}\right) dx.$$

The relation between the velocity components (u, v) and the stream function Ψ is given by

$$u = \frac{\partial \Psi}{\partial y}, v = -\frac{\partial \Psi}{\partial x}. \tag{24}$$

From (22) and (24), one can write

$$\Psi = \int u dy.$$

Numerical procedure

Using the command DSolve in the Mathematica program, linear Eqs. (17) and (18) were solved with boundary conditions (19). This procedure is useful in reducing CPU per evaluation as well as reducing error. Also, to obtain graphical solutions and numerical calculations, an appropriate algorithm has been developed for this matter.

Numerical results and discussion

This section discusses the graphical data that were found in this study for temperature, velocity, pressure gradient, pressure rise, friction forces, stress and streamlines. MATLAB is used for the simulation and the results are exhibited through graphs. For numerical computations, the material properties of parameter values as in Reddy⁴⁰ are taken under consideration. Figure 2 depict the impact of thermal radiation and heat source/sink on temperature with respect to y -axis, while keeping other parameters fixed. As increasing the parameter β the temperature increases, while it decreases when the value of the parameter R increasing. The temperature satisfies the boundary conditions. This result is in good agreement with the results obtained by Hayat et al.⁶.

Figure 3 displays the change in velocity u with the y -axis according to ϵ is the porosity of the porous medium, thermal radiation R , Gr Grashof number, M Hartmann number, heat source/sink β and Darcy's number Da . It can be seen that increasing Da, β, Gr and ϵ increases the velocity u , while rising R and M cause it to decrease. Moreover, it has the highest value in the channel's middle and the lowest value at the channel's edges. Also, it satisfies the boundary conditions. This is in good agreement with what was obtained in clinical practice because the nutrients diffuse out of the blood vessels to neighboring tissues²³.

Figure 4 illustrates the variations of the pressure gradient $\frac{dp}{dx}$ with respect to the x -axis for various parameters $Da, \beta, Gr, \epsilon, M$ and the phase difference ϕ . According to the graph, the pressure gradient rises when M, ϵ, Gr are increased while falling when Da, β, ϕ are decreased. it is observed that the pressure gradient oscillates in the whole range x . For more authenticity, this result is in good agreement with the results obtained by Reddy⁴⁰.

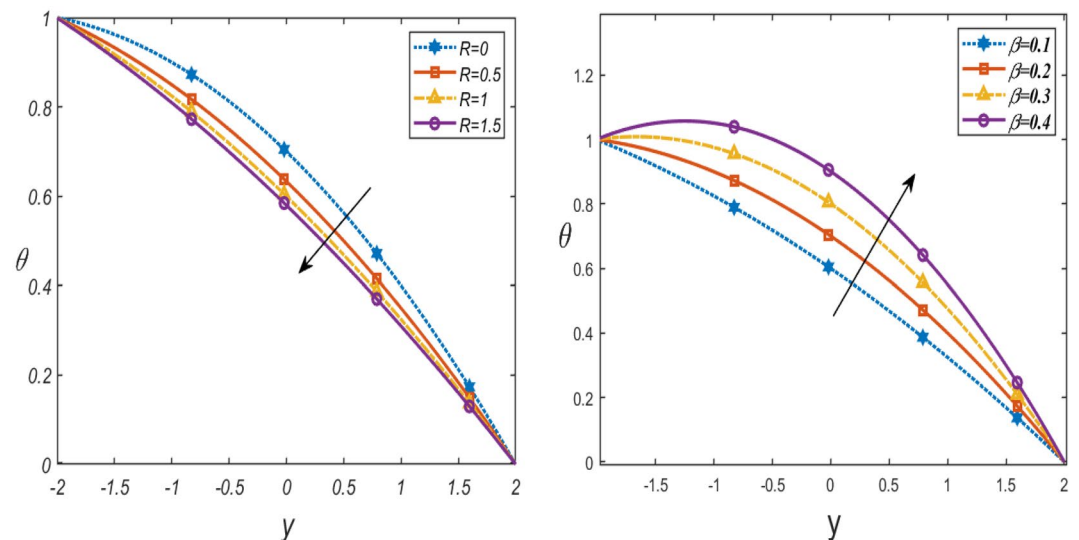


Figure 2. Changes of β, R on the temperature θ against y -axis.

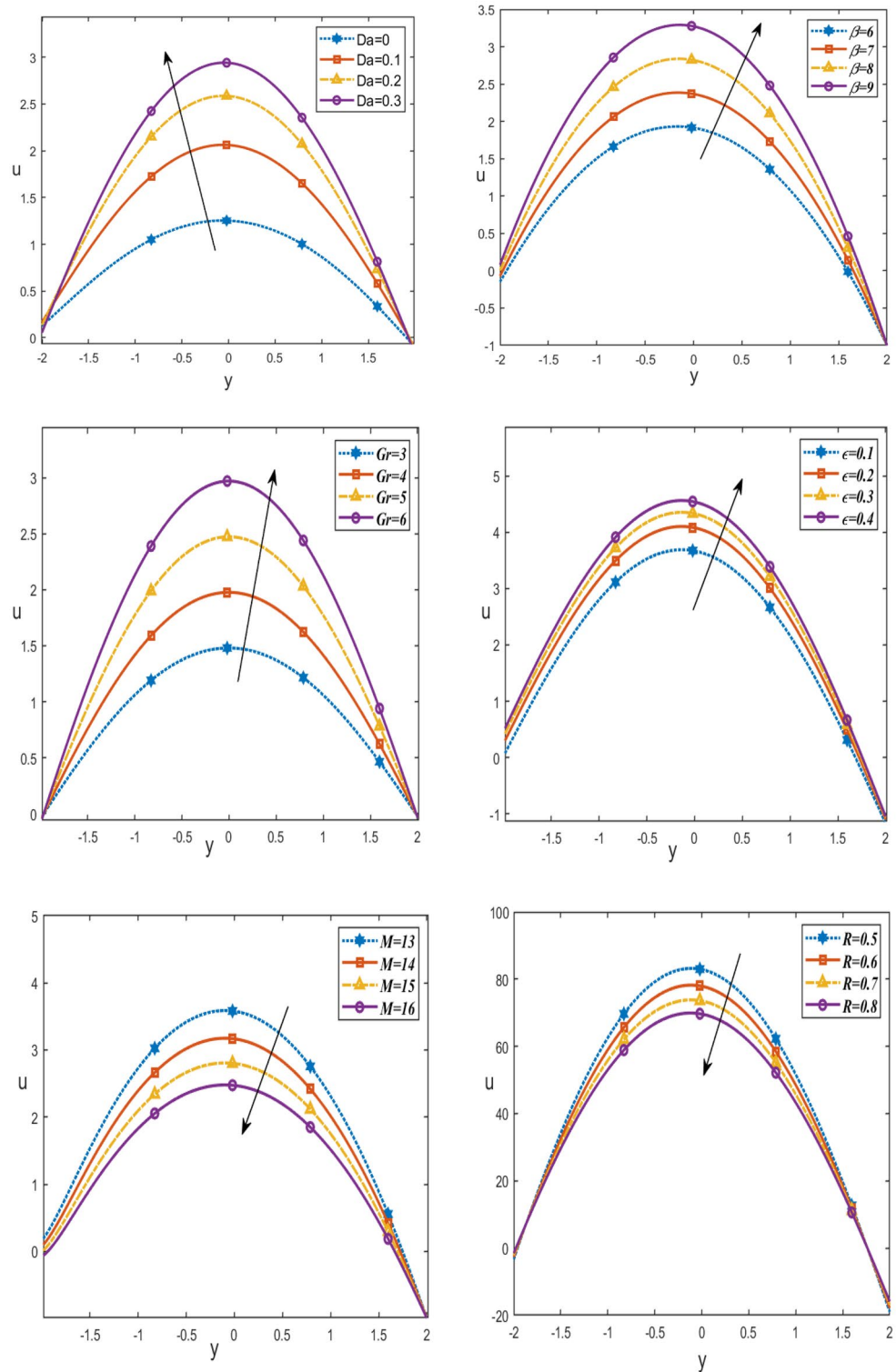


Figure 3. Changes of $Da, \beta, Gr, \epsilon, M, R$ on the velocity distribution u against y -axis.

Figure 5 presents the impact of $Da, \beta, Gr, \epsilon, M$ and ϕ on the pressure rise Δp_λ with respect to rate volume flow F . It is noticed that the pressure rise decreases with increasing β, Gr, ϵ , while it increases with increasing ϕ , as well, it increases with increasing M in the region $(-200 \leq F \leq 0)$ and it decreases in the interval $(0 \leq F \leq 200)$, otherwise it falls with rising Da in the period $(-200 \leq F \leq 0)$ and increases in the interval $(0 \leq F \leq 200)$. This result is in good agreement with the results obtained by Reddy⁴⁰.

Figures 6 and 7 demonstrate how the friction force for upper F_λ^u and lower F_λ^l varies with respect to a flow rate in volume F under these parameters $Da, \beta, Gr, \epsilon, M$. It is noticed that the friction force for lower and upper

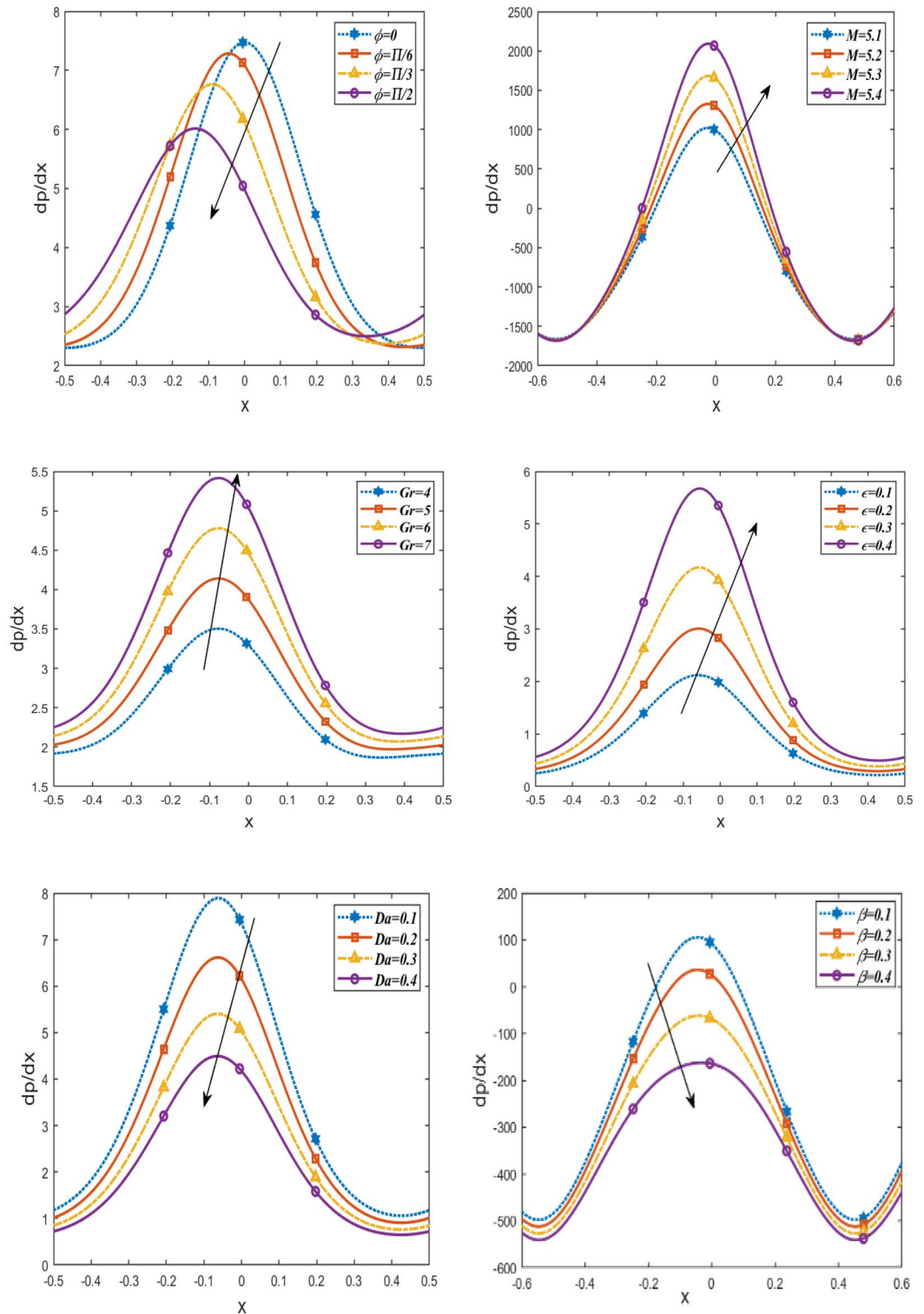


Figure 4. Changes of $Da, \beta, Gr, \epsilon, M, \phi$ on the pressure gradient $\frac{dp}{dx}$ against x -axis.

increases with increasing β, Gr, ϵ , as well, they increase with increasing Da in the interval $(-200 \leq F \leq 0)$ and decrease in the interval $(0 \leq F \leq 200)$. But by increasing M , they decrease in the interval $(-200 \leq F \leq 0)$ and increase in the interval $(0 \leq F \leq 200)$. The behavior of pressure rise is observed to be the inverse of the behavior of friction forces in the upper and lower layers. Figure 8 shows the variations of the shear stress τ_{xy} with respect to x -axis for different values of $\epsilon, Gr, M, \beta, R$ and Da . The stress decreases in the interval $(-0.5 \leq x \leq 0)$ and increases in the interval $(0 \leq x \leq 0.5)$ by rising Gr, Da , and β . While, it increases in the interval $(-0.5 \leq x \leq 0)$

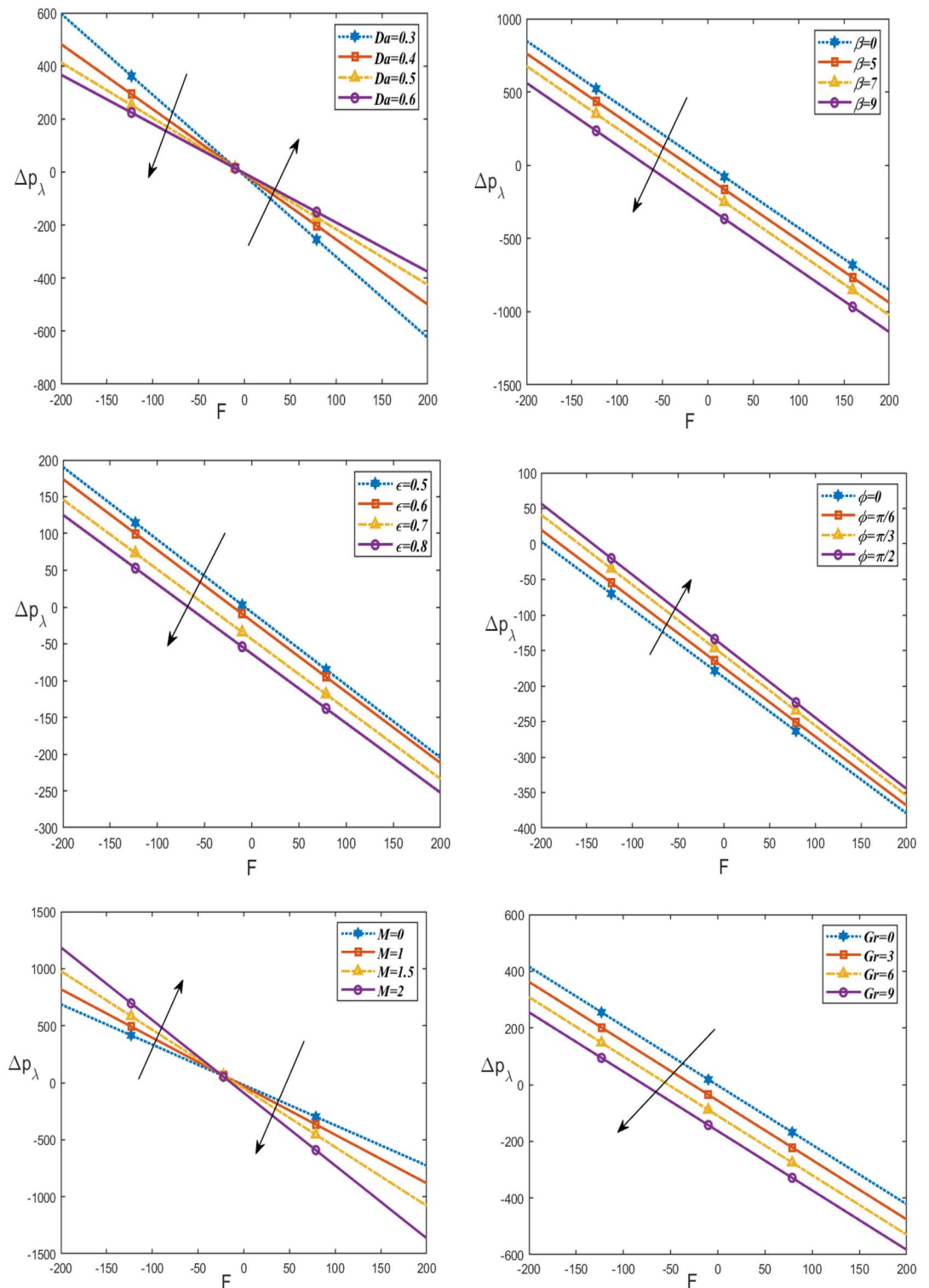


Figure 5. Changes of Da , β , $Gr\epsilon$, M , ϕ on the pressure rise Δp_λ against F .

and decreases in the interval $(0 \leq x \leq 0.5)$ by rising $g\epsilon$, R , M . Figure 9 shows the 3D schematics concern θ , u , and $\frac{dp}{dx}$, with regards to x and y axes under the effect of heat source β , Hartman number M , and Darcy number Da . The temperature is observed to drop as R increases, while the velocity increases with increasing Da and decreases with increasing M . Also, the pressure gradient decreases with increasing β . In 3D, all physical quantities derived from peristaltic flow overlap and dampen as they increase in order for particles to reach equilibrium. Most physical fields move in peristaltic flow, which is more relevant for the vertical distance of the curves that were created.

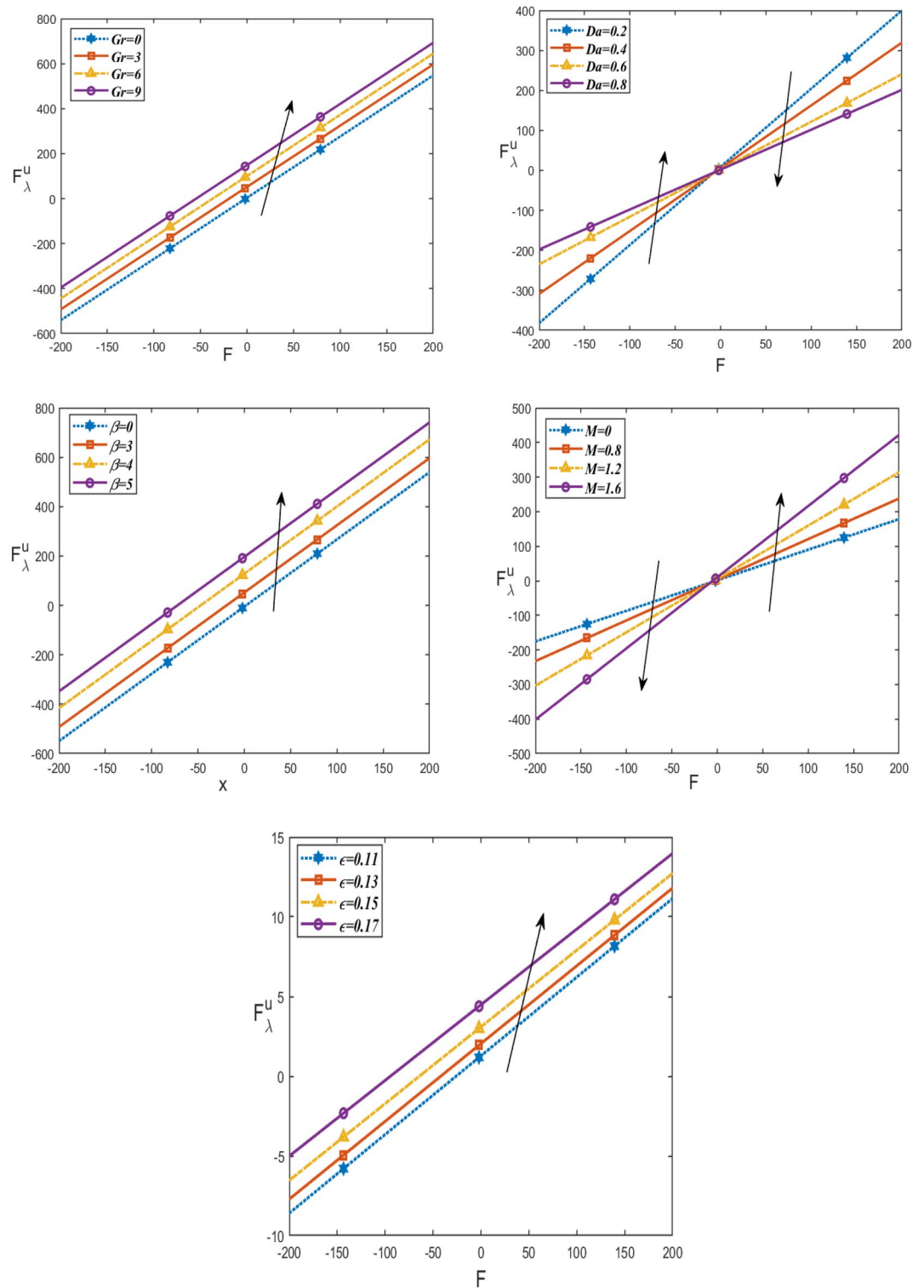


Figure 6. Changes of Da , β , Gr , ϵ , M on the friction force upper F_{λ}^u against F .

Streamlines pattern and trapping phenomenon

The peristaltic mechanism includes a study of the trapping phenomenon. Few streamlines shut during peristalsis, causing the creation of a bolus that circulates inside and advances at the rate of the peristaltic waves. This occurrence is known as trapping. Now, we will discuss this interesting case under the influence of some influences such as the heat source/sink β , the Grashof number Gr and the Hartman number M . Surprisingly, we observe that the trapping phenomenon occurs as shown in Fig. 10a–d, where it is when the value of the heat source/sink β increases that the bolus size decreases. In addition to, In Fig. 11a–d, it is seen that the boluses increase in size

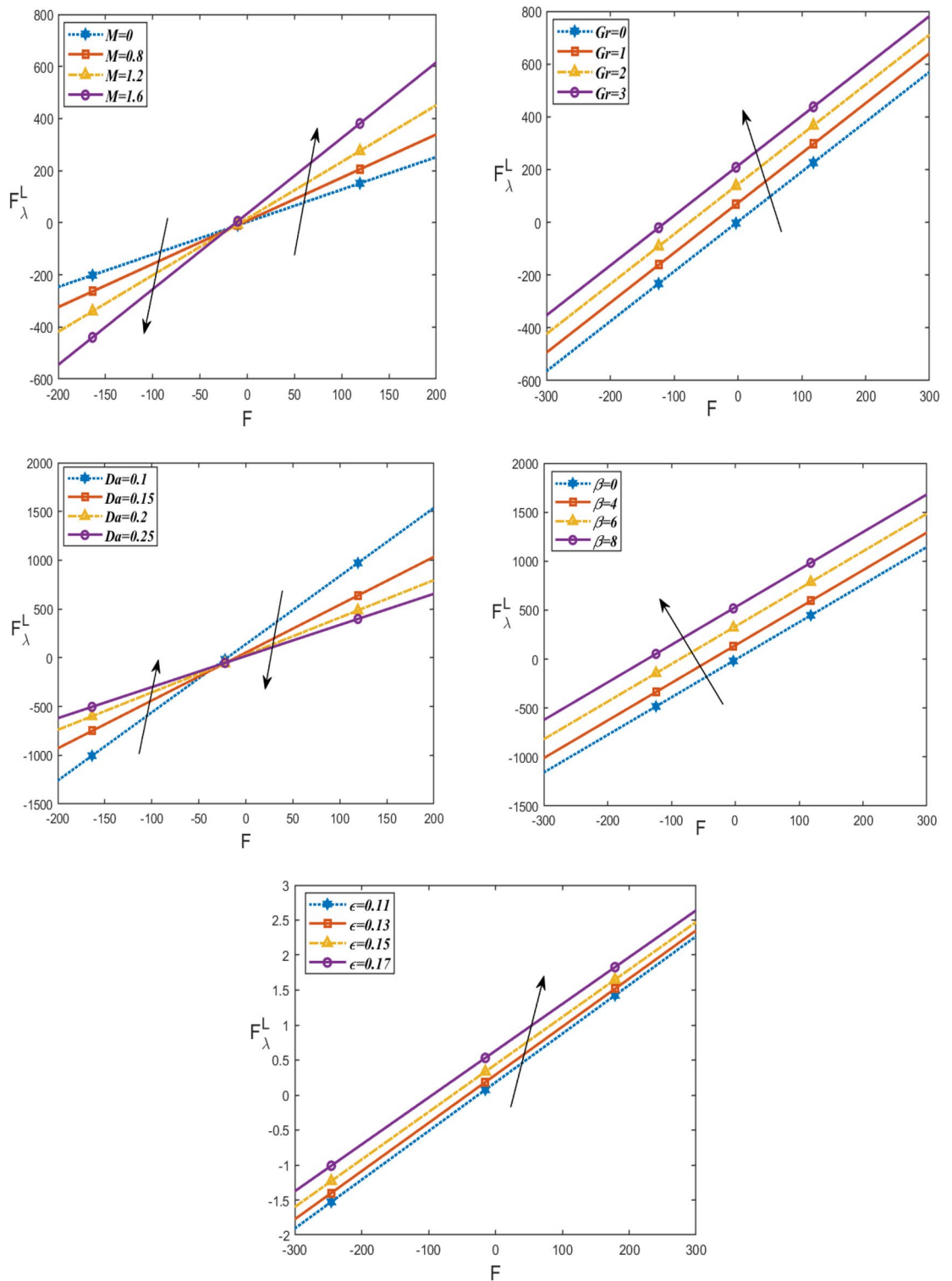


Figure 7. Changes of Da , β , Gr , ϵ , M on the friction force lower F_{λ}^L against F .

with increasing Gr . Also, we found that as M is raised, the trapped bolus's size grows, as shown in Fig. 12a–d. This increase in the size describes the volume of the fluid that is bounded by invariant closed streamlines. Furthermore, compared to the symmetric channel, the size of the trapped bolus is less in the asymmetric channel.

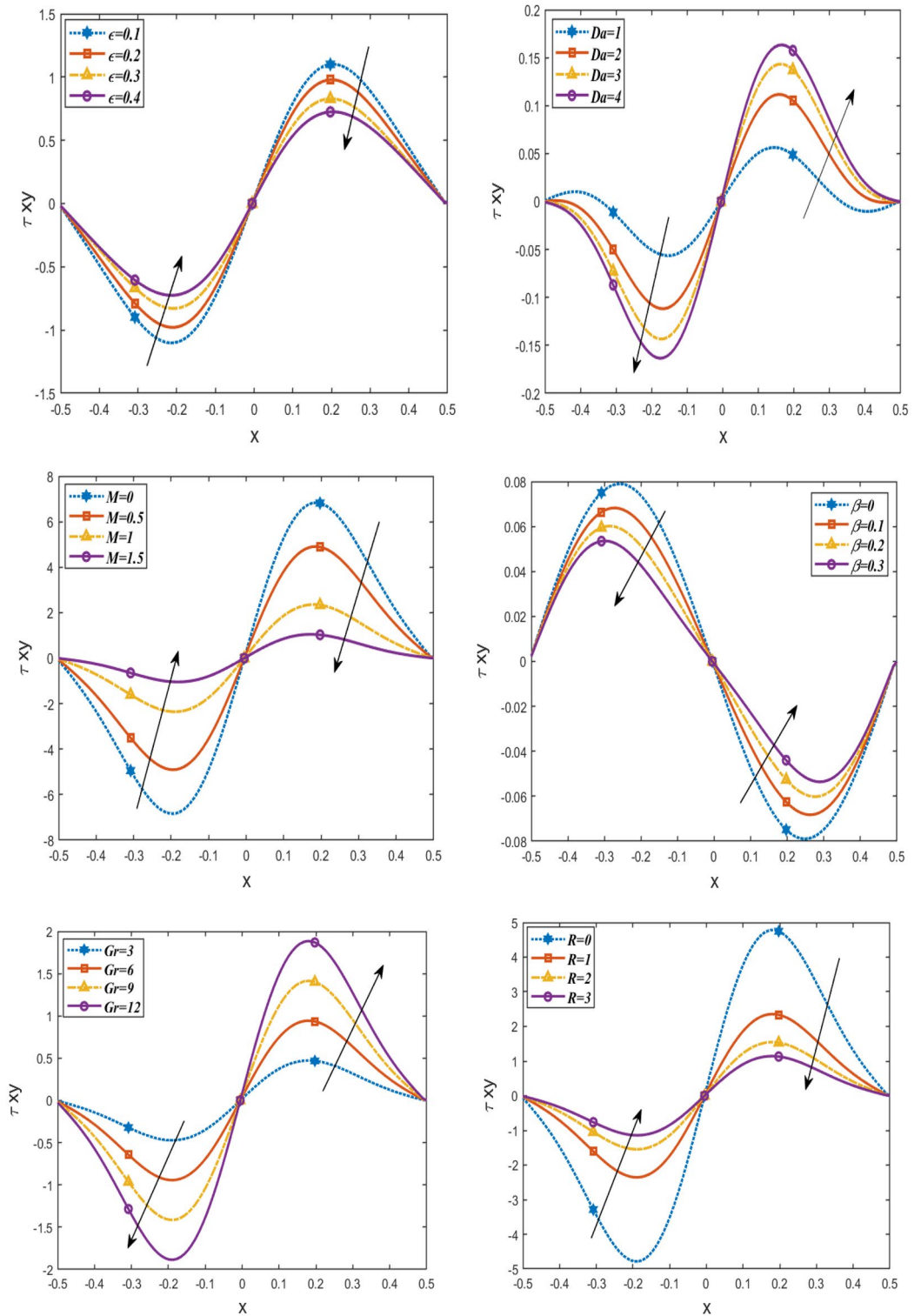


Figure 8. Changes of $Da, \beta, Gr\epsilon, M, \phi$ on the stress τ_{xy} against x -axis.

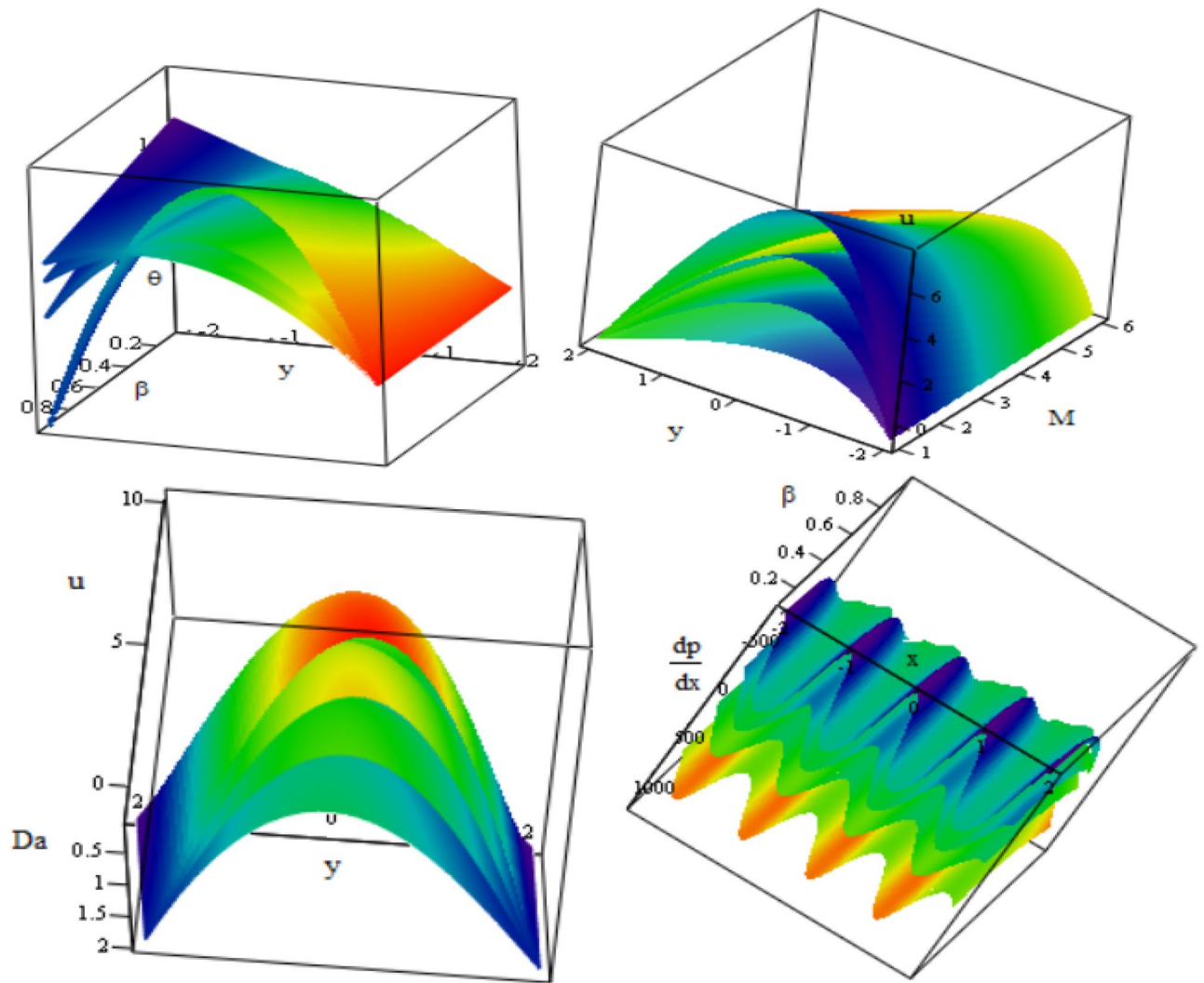


Figure 9. 3D plot of temperature θ , velocity u and the pressure gradient $\frac{dp}{dx}$ with x, y axes for changes in β, M and Da respectively.

Conclusion and future work

The role of the magnetic field and heat transfer have been studied for a fluid that is not Newtonian in a porous medium. To solve the problem mathematically, small Reynolds number and long wavelength assumptions are utilized. Graphical illustrations have been used to explain and discuss the impact of different physical factors on the flow characteristics. Below is a list of the important results.

- The partial differential equations that appear in this paper have an accurate analytical solution approach.
- Temperature can be increased by increasing β and reduced by increasing R .
- The flow has a maximum velocity in the centre and subsequently increases with increasing β, Da, Gr, ϵ and drops with increasing M, R , according to the graphical solutions for the velocity.
- The magnitude of pressure gradient has an oscillating behaviour as it increases by increments of M, Gr, ϵ and decreases by increments of Da, ϕ .
- Parameters Gr, ϵ, β have a decreasing effect on the pressure rise, while parameter ϕ has an increasing effect on it, as well, it increases with increasing M in the interval $-200 \leq F \leq 0$ and decreases in the interval $0 \leq F \leq 200$, otherwise it drops with raising Da in the period $-200 \leq F \leq 0$ and increases in the interval $0 \leq F \leq 200$.
- When compared to the pressure rise, the frictional force similarly has the opposite trend.
- The volume of the trapped bolus increases as the magnetic field and Grashof number increase, while it decreases as the heat source increases.
- Researchers working in the domains of science, engineering, medicine, and fluid mechanics may find the study's findings beneficial.
- Future research may be done in this approach to examine how slip circumstances affect flow characteristics.

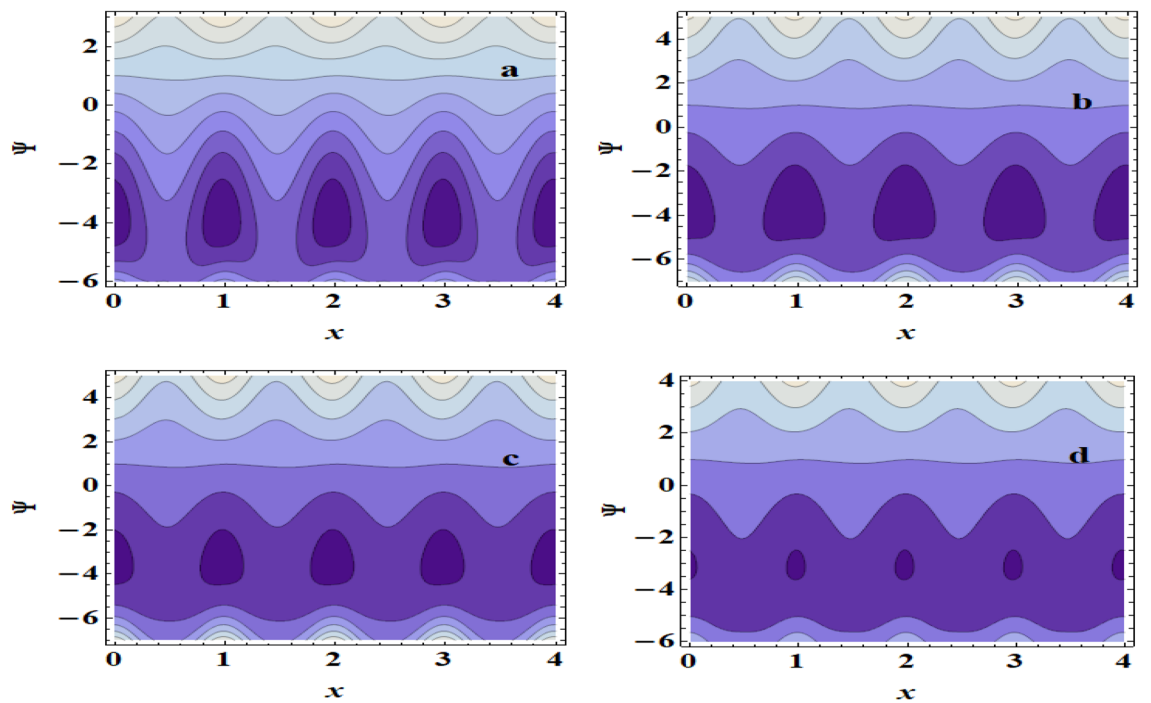


Figure 10. Streamlines for (a) $\beta = 0$, (b) $\beta = 0.1$, (c) $\beta = 0.3$, (d) $\beta = 0.5$.

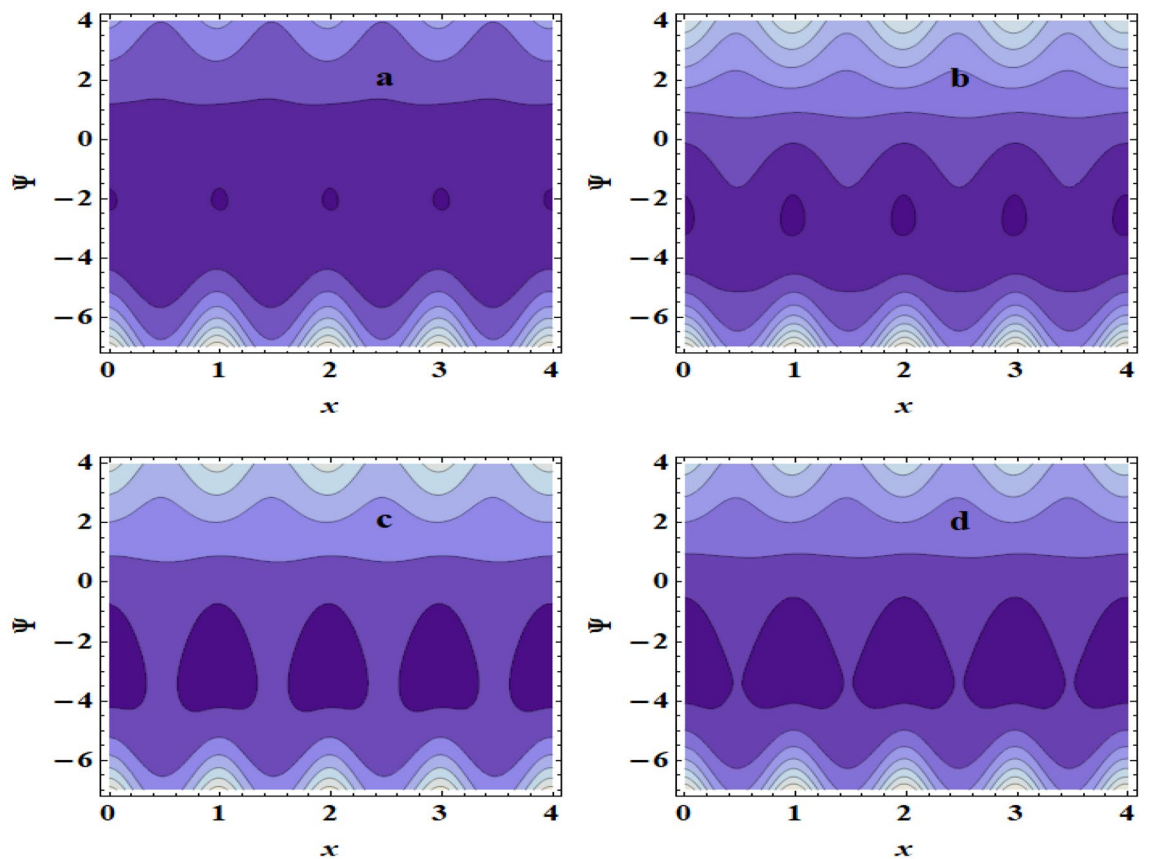


Figure 11. Streamlines for (a) $Gr = 1$, (b) $Gr = 3$, (c) $Gr = 5$, (d) $Gr = 7$.

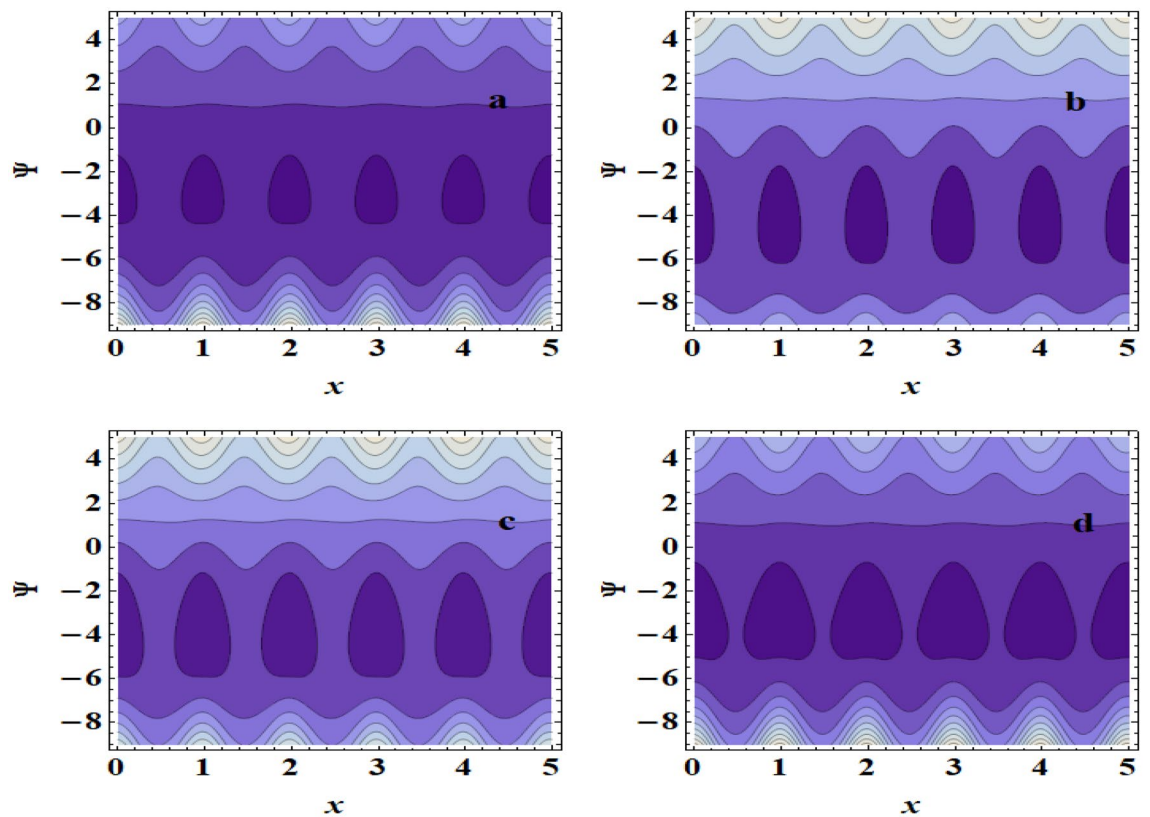


Figure 12. Streamlines for (a) $M = 0$, (b) $M = 0.1$, (c) $M = 0.5$, (d) $M = 0.8$.

Data availability

The datasets used and/or analyzed during the current study available from the corresponding author on reasonable request.

Received: 15 July 2023; Accepted: 23 October 2023

Published online: 30 November 2023

References

- Ealshahed, M. & Haroun, M. H. Peristaltic transport of Johnson-Segalman fluid under effect of a magnetic field. *Math. Probl. Eng.* **2005**, 663–667 (2005).
- Mekheimer, K. S. & Elmaboud, Y. A. The influence of heat transfer and magnetic field on peristaltic transport of a Newtonian fluid in a vertical annulus: Application of an endoscope. *Phys. Lett. A* **372**, 1657 (2008).
- Mekheimer, K. S. Peristaltic flow of a magnetomicrofluid: Effect of Induced magnetic field. *J. Appl. Math.* **2008**, 23 (2008).
- Mekheimer, K. S., Komyc, S. R. & Abdelsalamd, S. I. Simultaneous effects of magnetic field and space porosity on compressible Maxwell fluid transport induced by a surface acoustic wave in a microchannel. *Chin. Phys. B* **22**, 124702–212479 (2013).
- Hayat, T., Ali, N. & Asghar, S. Hall effects on peristaltic flow of a Maxwell fluid in a porous medium. *Phys. Lett. A* **363**, 397–403 (2007).
- Hayat, T., Qureshi, M. U. & Hussain, Q. Effect of heat transfer on the peristaltic flow of an electrically conducting fluid in a porous space. *Appl. Math. Model.* **33**, 1862–1873 (2009).
- Khan, A. A., Ellahi, R. & Vafai, K. Peristaltic transport of a Jeffrey fluid with variable viscosity through a porous medium in an asymmetric channel. *Adv. Math. Phys.* **2012**, 1–15 (2012).
- Hussain, Q., Asghar, S., Hayat, T. & AlSaed, A. Heat transfer analysis in peristaltic flow of MHD Jeffrey fluid with variable thermal conductivity. *Appl. Math. Mech.* **36**(4), 499–516 (2015).
- Latham, T. W. *Fluid Motions in a Peristaltic Pump*. M.S. Thesis. MIT (1966).
- Irshada, N., Saleemb, A., Nadeema, S. & Shahzadia, I. Endoscopic analysis of wave propagation with Ag-nanoparticles in curved tube having permeable walls. *Curr. Nanosci.* **14**, 384–402 (2018).
- Chakraborty, S. Augmentation of peristaltic microflows through electroosmotic mechanisms. *J. Phys. D Appl. Phys.* **39**(24), 53–56 (2006).
- Abbasi, A., Mabood, F., Farooq, W. & Khan, S. U. Radiation and joule heating effects on electroosmosis-modulated peristaltic flow of Prandtl nanofluid via tapered channel. *Int. Commun. Heat Mass Transf.* **123**, 105183 (2021).
- Akram, J., Akbar, N. S. & Maraj, E. N. A comparative study on the role of nanoparticle dispersion in electroosmosis regulated peristaltic flow of water. *Alexand. Eng. J.* **59**, 943–956 (2020).
- Mabood, F., Farooq, W. & Abbasi, A. Entropy generation analysis in the electro-osmosis modulated peristaltic flow of Eyring–Powell fluid. *J. Therm. Anal. Calorim.* **147**, 3815–3830 (2022).
- Shahzadi, I., Nadeem, S. & Rabiei, F. Simultaneous effects of single wall carbon nanotube and effective variable viscosity for peristaltic flow through annulus having permeable walls. *Results Phys.* **7**, 667–676 (2017).
- Shahzadi, I. & Nadeem, S. Impinging of metallic nanoparticles along with the slip effects through a porous medium with MHD. *J. Braz. Soc. Mech. Sci. Eng.* **39**, 2535–2560 (2017).

17. Shahzadi, I. & Nadeem, S. Inclined magnetic field analysis for metallic nanoparticles submerged in blood with convective boundary condition. *J. Mol. Liq.* **230**, 61–73 (2017).
18. Shahzadi, I. & Nadeem, S. Stimulation of metallic nanoparticles under the impact of radial magnetic field through eccentric cylinders: A useful application in biomedicine. *J. Mol. Liq.* **225**, 365–381 (2017).
19. Shahzadi, I. & Nadeem, S. Role of inclined magnetic field and copper nanoparticles on peristaltic flow of nanofluid through inclined annulus: Application of the clot model. *Commun. Theoret. Phys.* **67**(6), 704 (2017).
20. Shahzadi, I. & Nadeem, S. A comparative study of Cu nanoparticles under slip effects through oblique eccentric tubes, a biomedical solicitation examination. *Can. J. Phys.* **97**(1), 63 (2019).
21. Shahzadi, I., Suleman, S., Saleem, S. & Nadeem, S. Utilization of Cu-nanoparticles as medication agent to reduce atherosclerotic lesions of a bifurcated artery having compliant walls. *Comput. Methods Progr. Biomed.* **184**, 105123 (2020).
22. Ayub, M., Shahzadi, I. & Nadeem, S. A balloon model analysis with Cu-blood medicated nanoparticles as drug agent through overlapped curved stenotic artery having compliant walls. *Microsyst. Technol.* **25**(8), 2949–2962 (2019).
23. Li, S., Khan, M. I., Alzahrani, F. & Eldin, S. M. Heat and mass transport analysis in radiative time dependent flow in the presence of Ohmic heating and chemical reaction, viscous dissipation: An entropy modelling. *Case Stud. Therm. Eng.* **42**, 102722 (2023).
24. Li, S. *et al.* Analysis of the Thomson and Troian velocity slip for the flow of ternary nanofluid past a stretching sheet. *Sci. Rep.* **13**, 2340 (2023).
25. Xin, X., Khan, M. I. & Li, S. Scheduling equal-length jobs with arbitrary sizes on uniform parallel batch machines. *Open Math.* **31**, 20220562 (2023).
26. Jahanshahi, H., Yao, Q., Khan, M. I. & Moroz, I. Unified neural output-constrained control for space manipulator using tan-type barrier Lyapunov function. *Adv. Space Res.* **71**, 3712–3722 (2023).
27. Li, S. *et al.* Effects of activation energy and chemical reaction on unsteady MHD dissipative Darcy–Forchheimer squeezed flow of Casson fluid over horizontal channel. *Sci. Rep.* **13**, 2666 (2023).
28. Shahzadi, I. & Ijaz, S. On model of hybrid Casson nanomaterial considering endoscopy in a curved annulus: A comparative study. *Phys. Scr.* **94**, 125215 (2019).
29. Li, S. *et al.* Bioconvection effect in the Carreau nanofluid with Cattaneo–Christov heat flux using stagnation point flow in the entropy generation: Micromachines level study. *Open Phys.* **21**, 20220228 (2023).
30. Chu, Y.-M. *et al.* Double diffusion effect on the bio-convective magnetized flow of tangent hyperbolic liquid by a stretched nanomaterial with Arrhenius catalysts. *Case Stud. Therm. Eng.* **44**, 102838 (2023).
31. Liu, Z. *et al.* Numerical bio-convective assessment for rate type nanofluid influenced by Nield thermal constraints and distinct slip features. *Case Stud. Therm. Eng.* **44**, 102821 (2023).
32. Mamatha, S. U. *et al.* Multi-linear regression of triple diffusive convectively heated boundary layer flow with suction and injection: Lie group transformations. *Int. J. Mod. Phys. B* **37**(1), 2350007 (2023).
33. Shahzadi, I. & Kousar, N. Hybrid mediated blood flow investigation for atherosclerotic bifurcated lesions with slip, convective and compliant wall impacts. *Comput. Methods Progr. Biomed.* **179**, 104980 (2019).
34. Shahzadi, I. & Bilal, S. A significant role of permeability on blood flow for hybrid nanofluid through bifurcated stenosed artery: Drug delivery application. *Comput. Methods Progr. Biomed.* **187**, 105248 (2020).
35. Shahzadi, I., Duraihem, F. Z., Ijaz, S., Raju, C. S. K. & Saleem, S. Blood stream alternations by mean of electroosmotic forces of fractional ternary nanofluid through the oblique stenosed aneurysmal artery with slip conditions. *Int. Commun. Heat Mass Transf.* **143**, 106679 (2023).
36. Mekheimer, K. S., Shahzadi, I., Nadeem, S., Moawad, A. M. A. & Zaher, A. Z. Reactivity of bifurcation angle and electroosmosis flow for hemodynamic flow through aortic bifurcation and stenotic wall with heat transfer. *Phys. Scr.* **96**(1), 015216 (2020).
37. Sadaf, H. & Shahzadi, I. Physiological transport of Rabinowitsch fluid model with convective conditions. *Int. Commun. Heat Mass Transf.* **126**, 105365 (2021).
38. Nazir, U., Saleem, S., Al-Zubaidi, A., Shahzadi, I. & Feroz, N. Thermal and mass species transportation in tri-hybridized Sisko material with heat source over vertical heated cylinder. *Int. Commun. Heat Mass Transf.* **134**, 106003 (2022).
39. Kiranakumar, H. V. *et al.* A review on electrical and gas-sensing properties of reduced graphene oxide-metal oxide nanocomposites. *Biomass Convers. Biorefin.* <https://doi.org/10.1007/s13399-022-03258-7> (2022).
40. Reddy, M. G. Heat and mass transfer on magnetohydrodynamic peristaltic flow in a porous medium with partial slip. *Alexand. Eng. J.* **55**(2), 1225–1234 (2016).
41. Abdelhafez, M. A., Abd-Alla, A. M., Abo-Dahab, S. M. & Elmehdy, Y. Influence of an inclined magnetic field and heat and mass transfer on the peristaltic flow of blood in an asymmetric channel. *Sci. Rep.* **13**, 5749 (2023).
42. Abd-Alla, A. M., Abo-Dahab, S. M., Abdelhafez, M. A. & Elmehdy, Y. Effect of heat and mass transfer on the nanofluid of peristaltic flow in a ciliated tube. *Sci. Rep.* **13**, 16008 (2023).
43. Abd-Alla, A. M. *et al.* Effect of magnetic field and heat transfer on peristaltic flow of a micropolar fluid through a porous medium. *Waves Random Complex Media.* <https://doi.org/10.1080/17455030.2022.2058111> (2022).
44. Mohamed, R. A., Abo-Dahab, S. M., Abd-Alla, A. M. & Soliman, M. S. Magnetohydrodynamic double-diffusive peristaltic flow of radiating fourth-grade nanofluid through a porous medium with viscous dissipation and heat generation/absorption. *Sci. Rep.* **13**(1), 13096 (2023).
45. Abd-Alla, A. M., Abo-Dahab, S. M., Thabet, E. N., Bayones, F. S. & Abdelhafez, M. Heat and mass transfer in a peristaltic rotating frame Jeffrey fluid via porous medium with chemical reaction and wall properties. *Alexand. Eng. J.* **66**, 405–420. <https://doi.org/10.1016/j.aej.2022.11.016> (2023).
46. Abdelhafez, M. A., Abd-Alla, A. M., Abo-Dahab, S. M. & Elmehdy, Y. Influence of an inclined magnetic field and heat and mass transfer on the peristaltic flow of blood in an asymmetric channel. *Sci. Rep.* **13**, 5749. <https://doi.org/10.1038/s41598-023-30378-5> (2023).
47. Abd-Alla, A. M., Abo-Dahab, S. M., Abdelhafez, M. A. & Thabet, E. N. Effects of heat transfer and the endoscope on Jeffrey fluid peristaltic flow in tubes. *Multidiscip. Model. Mater. Struct.* **17**(5), 895–914 (2021).
48. Abd-Alla, A. M., Abo-Dahab, S. M. & Alsharif, A. M. Peristaltic transport of a Jeffrey fluid under the effect of gravity field and rotation in an asymmetric channel with magnetic field. *Multidiscip. Model. Mater. Struct.* **13**(4), 522–538 (2017).
49. Abd-Alla, A. M., Abo-Dahab, S. M. & Kilicman, A. Effect of radially varying MHD on the peristaltic flow in a tubes with an endoscope. *J. Magn. Magn. Mater.* **384**, 79–86 (2015).
50. Abd-Alla, A. M. & Abo-Dahab, S. M. Effect of rotation on peristaltic flow of fluid in a symmetric channel through a porous medium with magnetic field. *J. Comput. Theoret. Nanosci.* **12**(6), 934–943 (2015).
51. Abd-Alla, A. M. & Abo-Dahab, S. M. Effect of an endoscope and rotation on the peristaltic flow involving a Jeffrey fluid with magnetic field. *J. Braz. Soc. Mech. Sci. Eng.* **37**(4), 1277–1289 (2015).

Acknowledgements

The researchers would like to acknowledge Deanship of Scientific Research, Taif University for funding this work.

Author contributions

A.M.A.-A. suggest the idea of paper and appropriate ways to solve a problem and formulate the problem. S.M.A.-D. find the solution to the problem. M.A.A. explain the numerical results and find their physical meaning. D.M. S. wrote the paper and represented the numerical results graphically. F.S.B. revised and shear in discussion and conclusion.

Funding

Open access funding provided by The Science, Technology & Innovation Funding Authority (STDF) in cooperation with The Egyptian Knowledge Bank (EKB).

Competing interests

The authors declare no competing interests.

Additional information

Correspondence and requests for materials should be addressed to A.M.A.-A.

Reprints and permissions information is available at www.nature.com/reprints.

Publisher's note Springer Nature remains neutral with regard to jurisdictional claims in published maps and institutional affiliations.



Open Access This article is licensed under a Creative Commons Attribution 4.0 International License, which permits use, sharing, adaptation, distribution and reproduction in any medium or format, as long as you give appropriate credit to the original author(s) and the source, provide a link to the Creative Commons licence, and indicate if changes were made. The images or other third party material in this article are included in the article's Creative Commons licence, unless indicated otherwise in a credit line to the material. If material is not included in the article's Creative Commons licence and your intended use is not permitted by statutory regulation or exceeds the permitted use, you will need to obtain permission directly from the copyright holder. To view a copy of this licence, visit <http://creativecommons.org/licenses/by/4.0/>.

© The Author(s) 2023